Harriet C. Thoeny, MD
Frederik De Keyzer, MSc
Vincent Vandecaveye, MD
Feng Chen, MD
Xihe Sun, MD
Hilde Bosmans, PhD
Robert Hermans, MD, PhD
Eric K. Verbeken, MD, PhD
Chris Boesch, MD, PhD
Guy Marchal, MD, PhD
Willy Landuyt, PhD
Yicheng Ni, MD, PhD

Published online before print
10.1148/radiol.2372041638
Radiology 2005; 237:492–499

Abbreviations:
ADC = apparent diffusion coefficient
ROI = region of interest

[1] From the Departments of Radiology (H.C.T., F.D.K., V.V., F.C., X.S., H.B., R.H., G.M., Y.N.) and Pathology (E.K.V.), University Hospitals Leuven, Gasthuisberg, Herestraat 49, 3000 Leuven, Belgium; Departments of Diagnostic, Interventional and Pediatric Radiology (H.C.T.) and Clinical Research (C.B.), University Hospital of Bern, Inselspital, Bern, Switzerland; and Laboratory of Experimental Radiobiology/LEO, Catholic University Leuven, Leuven, Belgium (W.L.). Received September 23, 2004; revision requested November 26; revision received January 12, 2005; accepted February 1. H.C.T. supported by a grant from the Bernese Cancer League and by the Kurt and Senta Hermann Foundation. **Address correspondence to** R.H. (e-mail: *robert.hermans@uz.kuleuven.ac.be*).

Authors stated no financial relationship to disclose.

Author contributions:
Guarantors of integrity of entire study, H.C.T., R.H.; study concepts/study design or data acquisition or data analysis/interpretation, all authors; manuscript drafting or manuscript revision for important intellectual content, all authors; approval of final version of submitted manuscript, all authors; literature research, H.C.T., W.L., Y.N.; experimental studies, H.C.T., F.D.K., V.V., F.C., X.S., H.B., E.K.V., G.M., W.L., Y.N.; statistical analysis, F.D.K., C.B.; and manuscript editing, H.C.T., F.D.K., V.V., H.B., R.H., C.B., Y.N.

Effect of Vascular Targeting Agent in Rat Tumor Model: Dynamic Contrast-enhanced versus Diffusion-weighted MR Imaging[1]

PURPOSE: To compare dynamic contrast material–enhanced magnetic resonance (MR) imaging and diffusion-weighted MR imaging for noninvasive evaluation of early and late effects of a vascular targeting agent in a rat tumor model.

MATERIALS AND METHODS: The study protocol was approved by the local ethics committee for animal care and use. Thirteen rats with one rhabdomyosarcoma in each flank (26 tumors) underwent dynamic contrast-enhanced imaging and diffusion-weighted echo-planar imaging in a 1.5-T MR unit before intraperitoneal injection of combretastatin A4 phosphate and at early (1 and 6 hours) and later (2 and 9 days) follow-up examinations after the injection. Histopathologic examination was performed at each time point. The apparent diffusion coefficient (ADC) of each tumor was calculated separately on the basis of diffusion-weighted images obtained with low *b* gradient values (ADC_{low}; $b = 0$, 50, and 100 sec/mm^2) and high *b* gradient values (ADC_{high}; $b = 500$, 750, and 1000 sec/mm^2). The difference between ADC_{low} and ADC_{high} was used as a surrogate measure of tissue perfusion ($ADC_{low} - ADC_{high} = ADC_{perf}$). From the dynamic contrast-enhanced MR images, the volume transfer constant *k* and the initial slope of the contrast enhancement–time curve were calculated. For statistical analyses, a paired two-tailed Student *t* test and linear regression analysis were used.

RESULTS: Early after administration of combretastatin, all perfusion-related parameters (*k*, initial slope, and ADC_{perf}) decreased significantly ($P < .001$); at 9 days after combretastatin administration, they increased significantly ($P < .001$). Changes in ADC_{perf} were correlated with changes in *k* ($R^2 = 0.46$, $P < .001$) and the initial slope ($R^2 = 0.67$, $P < .001$).

CONCLUSION: Both dynamic contrast-enhanced MR imaging and diffusion-weighted MR imaging allow monitoring of perfusion changes induced by vascular targeting agents in tumors. Diffusion-weighted imaging provides additional information about intratumoral cell viability versus necrosis after administration of combretastatin.

Vascular targeting agents such as combretastatin are drugs that selectively lead to acute structural and functional changes in tumor vessels. These agents disrupt the vascular network in tumors and cause tumor cell death without damaging the vasculature of normal organs (1–3). The changes in tumor vessels occur rapidly and are reversible, with the extent of reversibility dependent on the dose of the agent used (4).

In contrast to treatment options such as radiation therapy or chemotherapy, vascular targeting agents are not expected to substantially reduce tumor size (5). Rather, intratumoral changes such as vascular shutdown and consequent increase in the necrotic tumor fraction are expected. Therefore, an assessment of the drug-induced intratumoral alterations is important for evaluation of tumor response to such therapy.

Investigators in preclinical studies (1,2,4) and phase I clinical trials (6–13) analyzed and monitored the effect of vascular targeting agents (eg, combretastatin A4 phosphate and 5,6-dimethylxanthenone-4-acetic acid) by using dynamic contrast material–enhanced magnetic resonance (MR) imaging, clinical and pharmacokinetic parameters, or scintigraphic methods (eg, positron emission tomography). Recently, diffusion-weighted MR imaging has been applied to monitor tumor response to therapy and has shown potential for helping to predict treatment outcome when used prior to initiation of chemotherapy (14).

Noninvasive techniques for monitoring the effects of vascular targeting agents are of utmost importance in the routine follow-up of cancer patients. Therefore, the aim of this study was to compare dynamic contrast-enhanced MR imaging with diffusion-weighted MR imaging for the noninvasive evaluation of early and late effects of a vascular targeting agent in a rat tumor model.

MATERIALS AND METHODS

Study Design

The study protocol was approved by the local ethics committee for animal care and use.

Experiments were performed in 13 adult (14-week-old) WAG/Rij male rats, each weighing 280–300 g. Two tumor sections (syngeneic, R1 rhabdomyosarcoma tumor cell line) from the same tumor, with each section having a volume of approximately 1 mm^3, were implanted (W.L.) subcutaneously in each rat, in the flank region on either side, at the level of the kidneys. Twenty-six tumors, with a mean volume of 3.49 $cm^3 \pm 1.19$ (range, 2.03–6.10 cm^3) before treatment, were analyzed. This tumor volume was reached at 2 weeks after implantation. There was a large degree of variability in volume because the two tumors in each rat did not grow at exactly the same rate.

Combretastatin A4 phosphate (Oxigene, Watertown, Mass) was administered intraperitoneally at a dose of 25 mg per kilogram of body weight. The first MR examination was performed 6 hours prior to drug administration (baseline). After intraperitoneal injection of combretastatin A4 phosphate, early (1 and 6 hours) and later (2 and 9 days) follow-up MR imaging examinations were performed. The entire study protocol was implemented in all rats except those that were sacrificed at each follow-up time point (four rats, one at each time point).

Histopathologic correlation was obtained by sacrificing one randomly selected rat (two tumors) from the group at each follow-up time point, and the remaining rats ($n = 9$) were sacrificed at the end of the experiments. For control, one rat underwent follow-up MR imaging 1 hour after intraperitoneal administration of saline solution at a volume identical to that of combretastatin A4 phosphate and was then sacrificed for histologic examination.

MR Imaging

The rats were examined in a 1.5-T whole-body MR imaging system (Sonata; Siemens, Erlangen, Germany) with a 40 mT/m maximum gradient capability. A four-channel phased-array wrist coil was used to obtain all MR images and allowed the use of parallel imaging techniques, with a generalized autocalibrating partially parallel acquisition, or GRAPPA, reduction factor of two in all cases. The rats were placed supine in a plastic holder for ease of fixation and injection of the contrast agent, and an inhaled anesthetic was used to avoid movement during imaging. Rats were initially anesthetized with inhalation of 4% isoflurane, and anesthesia was maintained with 2% isoflurane in a mixture of 20% oxygen and 80% room air. The animals were wrapped in towels to maintain body temperature. The penile vein was cannulated for intravenous access.

A coronal T1-weighted spin-echo sequence was used for tumor localization. A transverse T1-weighted spin-echo sequence (548/14 [repetition time msec/echo time msec], matrix of 120 × 256) then was applied with a section thickness of 2 mm, an intersection gap of 0.2 mm, and a parallel imaging reduction factor of two. The field of view was 81.3 × 130 mm to include both tumors in their entirety (20 sections), with a resultant voxel size of 0.7 × 0.5 × 2.0 mm. The acquisition time was 1 minute 32 seconds for the T1-weighted sequence, with two signals acquired.

Diffusion-weighted echo-planar MR imaging (3300/124, matrix of 57 × 128) was performed with a section thickness of 2 mm, an intersection gap of 0.2 mm, reduction factor of two, field of view of 81.3 × 130 mm, and 20 sections acquired, with a resultant voxel size of 1.4 × 1.0 × 2.0 mm. A range of *b* gradient values (in seconds per square millimeter) was used: $b = 0$, 50, 100, 150, 200, 250, 300, 500, 750, and 1000 sec/mm^2. These gradients were applied in each of three orthogonal directions and were combined to produce a trace data set to minimize the effects of diffusion anisotropy. The acquisition time was 2 minutes 35 seconds, with four signals acquired. Apparent diffusion coefficient (ADC) maps were calculated automatically by the MR imaging system. ADC was quantified in square millimeters per second.

Dynamic contrast-enhanced MR imaging was performed by using a three-dimensional T1-weighted gradient-echo sequence (volumetric interpolated breath-hold examination) with fat saturation (6.97/2.61, matrix of 96 × 192) and with a section thickness of 2 mm, reduction factor of two, field of view of 81.3 × 130 mm, and voxel size of 0.8 × 0.7 × 2.0 mm. For the entire volume of 20 sections, the acquisition time was 3.7 seconds with a single signal acquired. This sequence was applied continuously for 140 measurements (for a time equal to 140 × 3.7 seconds). After the first 15 measurements, an intravenous bolus of gadodiamide (Omniscan; Amersham, Oslo, Norway) with a gadolinium concentration of 0.5 mmol/mL was administered with a manual injection at a dose of 0.04 mmol/kg over a maximum period of 5 seconds. The results of a previous pilot study showed that this dose of contrast agent provides maximal signal enhancement with the same sequence used in this study. For all sequences, the parallel imaging reduction factor was applied in the phase-encoding direction.

Image Analysis

The image analysis was performed offline at a workstation by using dedicated LINUX-based software (Biomap; Novartis, Basel, Switzerland).

T1-weighted MR images.—Tumor volume was measured after the region of interest (ROI) was defined on transverse T1-weighted images. The entire tumor volume was manually delineated in each section by two observers (H.C.T., 7 years of experience in clinical MR imaging; F.D.K., 1 year of experience in experimental MR imaging) in consensus, and the dimensions of the individual sections were summed afterward. The ROIs were copied from the T1-weighted images to the ADC maps and the images obtained at volumetric interpolated breath-hold examinations at each follow-up time point.

Diffusion-weighted MR images.—The ROIs were copied from the ADC maps to the corresponding original diffusion-weighted images, from which the average

values for tumor signal intensity (averaged across all pixels in the ROI) for each *b* value were obtained. From the signal intensity averages per tumor and per *b* value, the ADC values of the tumors were calculated separately for low *b* values (b = 0, 50, and 100 sec/mm^2; ADC_{low}) and high *b* values (b = 500, 750, and 1000 sec/mm^2; ADC_{high}). From the literature, we know that ADC_{low} is influenced by diffusion, perfusion, and structural inhibitors, while ADC_{high} approximates the true diffusion coefficient (15). The ADC values were calculated by using least squares solutions to the following systems of equations:

For ADC_{low}: $S_i = S_0 \cdot \exp(-b_i \cdot ADC_{low})$ + NO, where S_i is the signal intensity measured on the diffusion-weighted image acquired with the *i*th low *b* value, S_0 represents the exact signal intensity (without the influence of noise induced by the MR measurement) with *b* equal to 0 sec/mm^2, b_i is the *i*th low *b* value (0, 50, and 100 sec/mm^2), and NO is noise. For ADC_{high}: $S_j = S_0 \cdot \exp(-b_j \cdot ADC_{high})$ + NO, where S_j is the signal intensity measured on the diffusion-weighted image acquired with the *j*th high *b* value, and b_j is the corresponding high *b* value (500, 750, and 1000 sec/mm^2). To reduce the influence of noise on the ADC calculations, diffusion-weighted images obtained with at least three different *b* values were used.

As a qualitative measure for tissue perfusion, the difference between ADC_{low} and ADC_{high} ($ADC_{low} - ADC_{high}$) was calculated and designated as ADC_{perf}. ADC_{perf} incorporates two parameters that are influenced by perfusion: the perfusion fraction and apparent diffusion caused by the incoherent motion of microcirculation (15).

Dynamic contrast-enhanced MR images.— For evaluation of the dynamic contrast-enhanced MR images, pixelwise contrast enhancement–time curves were calculated from the perfusion image series by using the following formula (16): $CTC_i = (I_i - I_0)/I_0$, for all time points *i*, where CTC_i is the contrast enhancement–time curve at time point *i*, I_i is the signal intensity at perfusion imaging at time point *i*, and I_0 is the signal intensity at baseline perfusion imaging. This formula defines the contrast in the tissue when a linear relation is assumed to exist between the amount of contrast agent in the tissue and the resulting difference in relaxation time R1 such that $C(t) = a \cdot \Delta R1$, where *t* indicates the time after contrast agent administration. This assumption holds true when low doses of a gadolinium-based contrast agent are used, as in the present study (17).

The arterial input function was assessed by placing an additional ROI in the aorta. From this ROI, the concentration of gadodiamide in the blood plasma (C_p) was extracted. For the ROIs in the tissue, the Tofts and Kermode model (17) was then used to calculate the volume transfer constant *k* (in 1/sec) according to the following formula, which is based on the assumption that the permeability of tumor vessels for contrast agent flow from intravascular to extracellular extravascular space is identical to their permeability for flow from extracellular extravascular to intravascular space:

$$\frac{dC_t}{dt} = -\frac{k}{V_e} C_t + k\left(1 + \frac{V_p}{V_e}\right) C_p + V_p \frac{dC_p}{dt}.$$

The volume transfer constant *k* is the permeability–surface area product per unit of tissue volume. This value is now generally known as K_{trans}; however, because of small deviations in absolute value due to the assumptions made, we continue to use the denomination *k*. C_t is the concentration of contrast agent in the tumor tissue, which is assumed to be represented by the previously determined contrast enhancement–time curve. V_e and V_p are the volumes per unit of tumor tissue belonging to the extracellular extravascular space and blood plasma, respectively. As V_p and V_e have not been used regularly in the literature, only the results for the volume transfer constant *k* are reported.

Further evaluation was performed by calculating the slope of the contrast enhancement–time curve at the time point of maximal contrast agent inflow, which was defined as the initial slope (IS): IS = max[d(CTC)/dt].

Comparison of Diffusion-weighted with Dynamic Contrast-enhanced MR Images

ADC_{high} reflects almost only diffusion, whereas ADC_{low} indicates both diffusion and perfusion (15). Therefore, we designated the difference between ADC_{low} and ADC_{high} as ADC_{perf} ($ADC_{perf} = ADC_{low} - ADC_{high}$), because this difference is assumed to correspond mainly to perfusion. That assumption was confirmed by the results of a pilot study in which we analyzed diffusion-weighted MR images of rat kidneys before and after sacrifice (unpublished data, F.D.K., 2004). Values for ADC_{perf} were compared with those for the volume transfer constant *k* and the initial slope of the contrast enhancement–time curve for the different tumors and for time points before and after combretastatin administration.

Histologic Analysis and Comparison with MR Images

After surgical excision at the time points mentioned earlier, tumors were fixed in 10% formaldehyde solution and sliced in sections approximately 2 mm thick in the transverse plane that corresponded to the dimensions of the MR sections. The sections were embedded in paraffin and were sliced further into 5-μm-thick sections, which were stained with hematoxylin and eosin. All sections were examined with light microscopy by an experienced pathologist (E.K.V., 20 years of experience) using a magnification of ×12.5 to ×400. Tissue sections were microscopically assessed for the presence and extent of viable tumor cells, necrosis, and changes of the intratumoral vasculature (such as vessel constriction, congestion, and dilatation). Thereafter, the histologic sections were compared visually with the corresponding transverse spin-echo images and the transverse ADC maps at the midlevel of the tumor (18).

Statistical Analysis

Statistical analysis was performed by using software (Excel 9.0, Microsoft, Seattle, Wash; Analyze-It 1.68, Leeds, England). Numeric data are reported as the mean ± standard deviation. For statistical comparison of values obtained at two consecutive time points for the initial slope of the contrast enhancement–time curve, the volume transfer constant *k*, and ADC_{perf}, paired two-tailed Student *t* tests were performed. ADC_{perf} was compared with *k* and the initial slope by using linear regression analyses to determine whether the parameters were correlated. A *P* value of less than .05 was considered to indicate a significant difference. Data obtained in different tumors in the same rat were treated as independent measures because previous examinations showed no correlation between data from the two tumors in each rat, either in the findings on baseline images or in the tumor response.

RESULTS

T1-weighted MR Images

The tumor volumes calculated from measurements on the T1-weighted images are shown in Figure 1. Before treatment, the mean tumor volume was 3.49

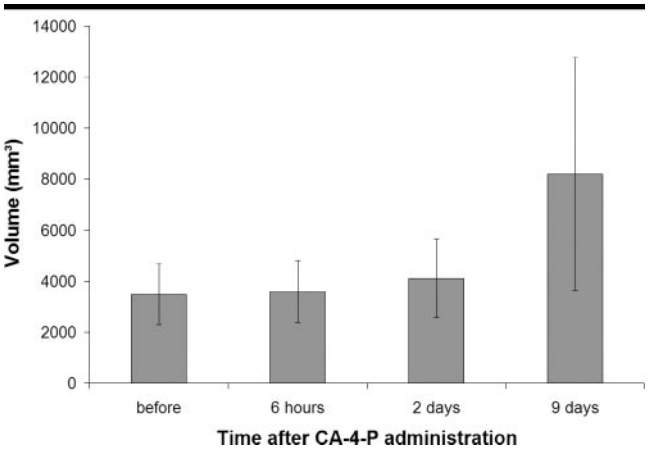

Figure 1. Graph shows mean tumor volume before and at three time points after combretastatin *(CA-4-P)* administration, as measured on transverse T1-weighted images. Whiskers indicate the standard deviation.

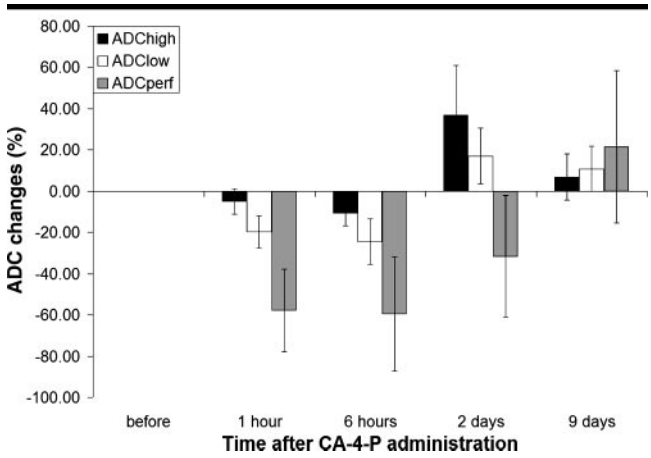

Figure 2. Graph shows change (as a percentage) in ADC_{low} (b = 0, 50, and 100 sec/mm^2), ADC_{high} (b = 500, 750, and 1000 sec/mm^2), and ADC_{perf} (ADC_{low} − ADC_{high}) over time after injection of combretastatin *(CA-4-P)*, compared with mean values at baseline. Whiskers indicate the standard deviation.

cm^3 ± 1.19. Six hours later, no significant change was found (3.60 cm^3 ± 1.20, P = .11). Two days later, the tumors had grown significantly, to 4.11 cm^3 ± 1.54 (P = .01). Further significant growth, to 8.21 cm^3 ± 4.56 (P < .001), was observed at 9 days.

Diffusion-weighted MR Images

Changes in mean values of ADCs (ADC_{low}, ADC_{high}, and ADC_{perf}) over time after intraperitoneal injection of combretastatin A4 phosphate, with averaging of ADC values over the entire tumor volume and with expression of change as a percentage of the baseline value, are shown in Figure 2 and in the Table. The Table also shows the P values for comparisons between consecutive time points.

A marked decrease in ADC_{low} was observed 1 hour after combretastatin injection (P < .001), compared with the same parameter at baseline. A further decrease, measured at 6 hours after the injection, was less pronounced but still significant (P = .004). At 2 days after combretastatin injection, ADC_{low} increased significantly (P < .001), and then it decreased slightly at 9 days after (P = .13).

ADC_{high} decreased at early follow-up examinations (1 and 6 hours, P = .005 and P < .001, respectively) after combretastatin administration. A significant increase was noted between the follow-up examinations at 6 hours after and 2 days after combretastatin injection (P < .001). At 9 days after injection, a significant decrease (P < .001) again was observed.

ADC_{perf} decreased significantly in the 1st hour after combretastatin administration (P < .001) and remained stationary at 6 hours after (P = .76). It increased between the follow-up examinations at 6 hours after and 2 days after (P = .004) and increased further at 9 days after (P < .001) combretastatin injection (Figs 2, 3).

Dynamic Contrast-enhanced MR Images

Figure 3 shows changes in the volume transfer constant k and the initial slope of the contrast enhancement–time curve over time after combretastatin administration, compared with changes in ADC_{perf} at the same time points.

Both the volume transfer constant k and the initial slope were significantly decreased at 1 hour (P < .001 for both) and slightly decreased at 6 hours (P = .19, and P = .66) after combretastatin administration. Between the examinations at 6 hours after and at 2 days after combretastatin injection, the volume transfer constant k increased slightly (P = .07), but the initial slope increased significantly (P = .005). A significant increase in both parameters was observed also from 2 days to 9 days after combretastatin injection (initial slope: P = .006; volume transfer constant k: P = .003) (Fig 4).

Comparison between Diffusion-weighted and Dynamic Contrast-enhanced MR Images

The results of the two linear regression analyses—both that in which ADC_{perf} was compared with the volume transfer constant k and that in which ADC_{perf} was compared with the initial slope of the contrast enhancement–time curve—showed a significant difference (P < .001), with R^2 values of 0.46 and 0.67, respectively.

Histopathologic Analysis

Results of histopathologic analysis of tumor specimens from the control rat showed a central necrotic area completely surrounded by a thick peripheral layer of viable tumor cells, with many mitoses. The periphery was sharply demarcated from the necrotic center.

The corresponding histologic specimens taken 1 and 6 hours after intraperitoneal injection of combretastatin showed central necrosis at both time points. At 1 hour, constriction of the vessels in the periphery, with evidence of still-viable tumor cells, could be observed. Six hours after combretastatin administration, edema was present. The blood vessels were dilated and/or congested. Tumor cells, however, remained viable. No evidence of hemorrhage was seen at histologic analysis. At 2 days after combretastatin administration, histologic examination demonstrated extensive enlargement of the necrotic area and only a small rim of viable tumor tissue and normal noncongested vessels remaining at the outer periphery. At 9 days, histologic analysis revealed regrowth of solid tumor at the periphery, with an increased number of blood vessels.

DISCUSSION

These data indicate that dynamic contrast-enhanced MR imaging and diffu-

Comparison of Calculated Parameters before and at Four Time Points after Administration of Combretastatin

Parameter	6 Hours Before	1 Hour After	6 Hours After	2 Days After	9 Days After
ADC_{high}*					
Absolute value (mm^2/sec)	0.00120 ± 0.00013	0.00114 ± 0.00013	0.00107 ± 0.00012	0.00163 ± 0.00024	0.00128 ± 0.00017
Change (%)		−5.01 ± 6.10	−10.63 ± 6.22	+36.98 ± 23.89	+6.86 ± 11.18
P value		.005	<.001	<.001	<.001
ADC_{low}†					
Absolute value (mm^2/sec)	0.00166 ± 0.00017	0.00133 ± 0.00016	0.00125 ± 0.00018	0.00194 ± 0.00025	0.00184 ± 0.00024
Change (%)		−19.79 ± 7.77	−24.42 ± 11.10	+17.09 ± 13.48	+10.77 ± 10.94
P value		<.001	.004	<.001	.126
ADC_{perf}‡					
Absolute value (mm^2/sec)	0.00046 ± 0.00009	0.00019 ± 0.00008	0.00018 ± 0.00011	0.00031 ± 0.00012	0.00056 ± 0.00019
Change (%)		−57.80 ± 19.99	−59.46 ± 27.64	−31.59 ± 21.51	+21.51 ± 36.84
P value		<.001	.760	.004	<.001
k (1/sec)					
Absolute value (mm^2/sec)	0.0489 ± 0.0283	0.0097 ± 0.0084	0.0061 ± 0.0089	0.0171 ± 0.0189	0.0541 ± 0.0452
Change (%)		−72.35 ± 33.26	−79.24 ± 33.00	−51.44 ± 58.81	+36.85 ± 90.99
P value		<.001	.189	.069	.003
Initial slope					
Absolute value (mm^2/sec)	0.0745 ± 0.0201	0.0150 ± 0.0092	0.0146 ± 0.0113	0.0276 ± 0.0172	0.0510 ± 0.0205
Change (%)		−77.73 ± 16.13	−78.61 ± 18.57	−60.23 ± 29.32	−30.83 ± 24.85
P value		<.001	.664	.005	.006

Note.—Data are the mean ± standard deviation unless otherwise indicated. *P* values were calculated by using paired two-tailed Student *t* tests for comparison of values at two consecutive time points.

* ADC_{high} = ADC on diffusion-weighted MR images obtained with high *b* gradients (*b* = 500, 750, and 1000 sec/mm^2).

† ADC_{low} = ADC on diffusion-weighted MR images obtained with low *b* gradients (*b* = 0, 50, and 100 sec/mm^2).

‡ ADC_{perf} = perfusion-associated ADC, calculated by subtracting ADC_{high} from ADC_{low}.

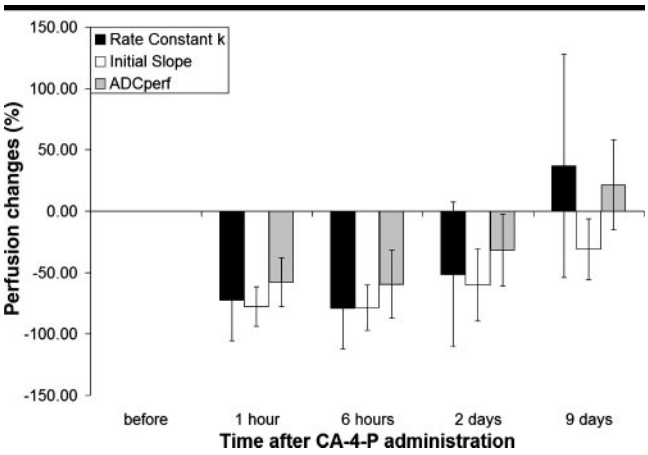

Figure 3. Graph shows change (as a percentage) over time, after intraperitoneal injection of combretastatin *(CA-4-P)*, in mean values for ADC_{perf} calculated from the diffusion-weighted MR images and in the volume transfer constant *k* and initial slope of the contrast enhancement–time curve calculated from dynamic contrast-enhanced MR images. Whiskers indicate the standard deviation.

sion-weighted MR imaging both depict distinctive early and late changes in tumors after administration of a vascular targeting agent. At the same time points, changes in viable tumor tissue and blood vessels were documented at histologic analysis.

Dynamic contrast-enhanced MR imaging is a valid method for monitoring the effectiveness of a variety of treatments, including chemotherapy, hormonal manipulation, radiation therapy, and drug therapy with new antiangiogenic agents and vascular targeting agents (6,13,19, 20). Dynamic contrast-enhanced MR imaging is a noninvasive technique for measurement of parameters that are related to tissue perfusion and permeability (21,22). High first-pass extraction of low-molecular-weight contrast medium results in the domination of the volume transfer constant *k* by tissue perfusion. There are a few tissues in which the volume transfer constant is dominated by the permeability–surface area product. As a corollary, in tumors that are not treated with combretastatin A4 phosphate, the volume transfer constant is dominated by perfusion, whereas the volume transfer constant in the treated tumors is dominated by the permeability–surface area product. Diffusion-weighted MR imaging has been used to predict and monitor the effect of several treatment options (18,23, 24) and to differentiate between viable and necrotic tumor tissue in an animal model of untreated osteogenic sarcoma (25). This MR imaging technique enables the depiction of molecular diffusion, which is the brownian motion of the water protons in biologic tissues (15). The calculation of the ADC allows the quantification of that motion. When only high *b* values are used at diffusion-weighted imaging, the ADC approximates the true diffusion coefficient of the tissue in question; when only low *b* values are applied, the ADC value is influenced also by perfusion (15). Therefore, we assume that the difference between the ADC calculated from images obtained with low *b* values versus that calculated from images obtained with high *b* values likely reflects mainly perfusion. Since the perfusion fraction in ADC_{perf} is intermingled with the influence of perfusion on the ADC, only a complex relation between ADC_{perf} and dynamic contrast-enhanced MR imaging can be assumed, a relation in which perfusion is dominated

by the volume transfer constant *k*. The results described, however, seem to justify this assumption.

Confirming previously published data, our results demonstrate that dynamic contrast-enhanced MR imaging enables monitoring of the effects of a vascular targeting agent on tumors (5–7). To our knowledge, however, no correlation of dynamic contrast-enhanced MR imaging with diffusion-weighted MR imaging previously was performed in this specific cancer treatment model.

In the early phase after the administration of combretastatin, initial decreases in ADC_{perf}, the volume transfer constant *k*, and the initial slope were paralleled by a decrease in enhancing areas on the T1-weighted contrast-enhanced images. These findings represented evidence of vascular shutdown observed at histologic analysis. ADC_{high}, however, changed only slightly during the first 6 hours, with the change corresponding to the presence of nonperfused but histologically still viable tumor tissue.

At 2 days after combretastatin administration, small but significant increases in ADC_{perf} and the initial slope and a slight increase in the volume transfer constant *k* indicated early tumor regrowth. A possible explanation might be that new vessels in the tumor periphery were not yet very permeable; in addition, co-opted normal host vasculature at the edge of tumor expansion may be involved. As ADC_{perf} most probably reflects microcirculation and is not an indicator of permeability (22), this parameter increases, while the volume transfer constant *k*, which also reflects permeability, is not yet affected. All parameters increased significantly at 9 days, corresponding to extensive histologic evidence of peripheral tumor regrowth. ADC_{high} increased significantly between 6 hours and 2 days after combretastatin injection, a change that corresponded to an increase in the necrotic tumor fraction. The subsequent decrease in ADC_{high} indicates progressive regrowth of solid tumor as seen at histologic analysis.

Our results show a significant acute reduction in perfusion and, thus, corroborate previously published data about the effects of combretastatin on rat tumors at 1 and 6 hours after administration (1,5,26). In our investigation, this decrease in perfusion was demonstrated with dynamic contrast-enhanced MR imaging as well as with diffusion-weighted MR imaging. Prise et al (26) observed an 85% decrease in blood flow 1 hour after administration of 30 mg/kg of combretastatin A4 phosphate in P22 carcinosarcoma–bearing rats by using radiolabeled iodoantipyrine. A similar initial decrease in the volume transfer constant *k* by 72% after administration of a slightly smaller dose of combretastatin was observed in our study. In another investigation of a rat P22 carcinosarcoma (27), the value of the volume transfer constant between blood plasma and extracellular extravascular space was reduced by 64% at 6 hours after treatment with 30 mg/kg combretastatin A4 phosphate (7). ADC_{perf} in our investigation decreased by 59%, whereas the initial slope was reduced by 79% at this same time point. Although all reported perfusion changes after combretastatin administration are of the same order, the observed differences can be attributed to varying tumor models, contrast agent and combretastatin doses, and/or methods applied for monitoring the antitumor effect.

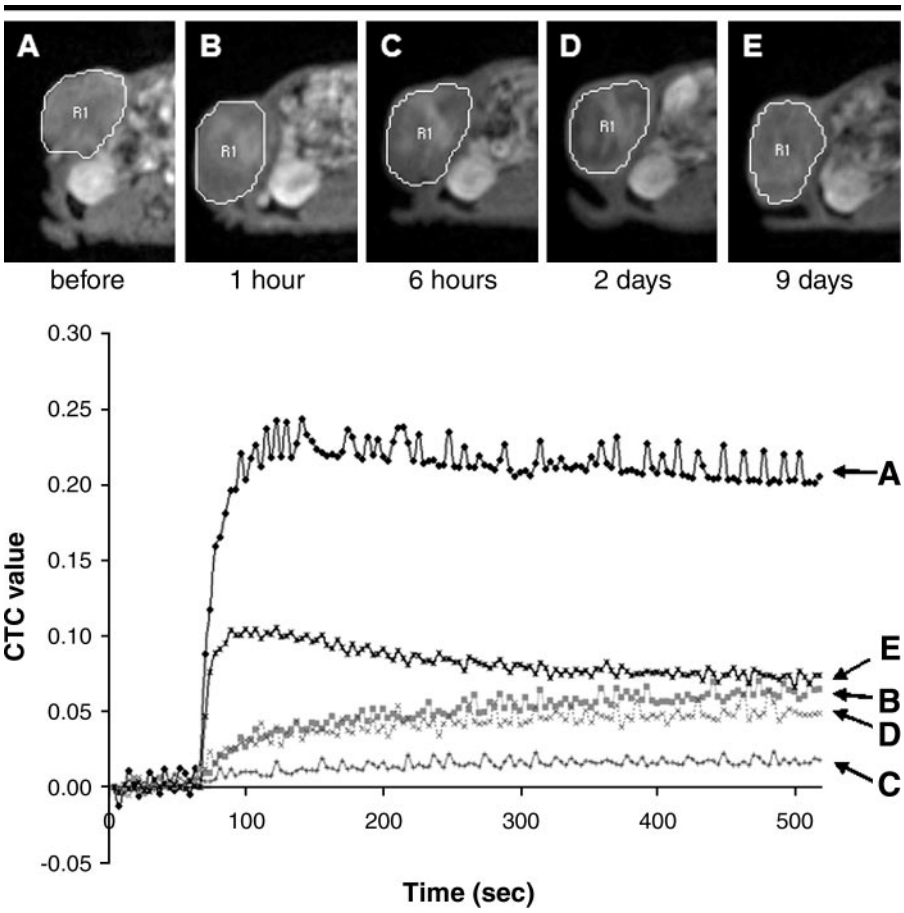

Figure 4. Top: Transverse dynamic contrast-enhanced MR images acquired in a randomly chosen tumor (subcutaneous rat rhabdomyosarcoma), after the first pass of the contrast medium bolus (at 120 sec), during volumetric interpolated breath-hold examinations (6.97/2.59) 6 hours before *(A)* and 1 hour, 6 hours, 2 days, and 9 days after *(B–E)* combretastatin injection. Change in contrast enhancement over time is difficult to appreciate visually. Bottom: Corresponding graph of contrast enhancement–time curves *(CTC)* shows that the initial slope is much lower in *B–D* than in *A* and *E*.

Our results demonstrate linear correlations of ADC_{perf} with the volume transfer constant *k* and the initial slope as calculated from the dynamic contrast-enhanced MR images.

The time-course of changes in *k* and in the initial slope measured on dynamic contrast-enhanced MR images and in ADC_{perf} calculated from diffusion-weighted MR images after combretastatin administration was similar in the early period (at 1 and 6 hours), although the relative changes in ADC_{perf} were smaller than those in the volume transfer constant *k*. Thus, the use of diffusion-weighted MR images (and ADC_{perf}) to measure change in tumor vessel blood flow after combretastatin administration leads to an underestimation of microcirculatory change. This underestimation is probably due to the effect of permeability

changes on the *k* value and the initial slope.

The calculated values of ADC_{perf}, ADC_{high}, and the initial slope increased significantly at 2 days, whereas the volume transfer constant *k* increased only slightly. The increase in ADC_{high} corresponds to an increase in the necrotic tumor fraction. The increase in ADC_{perf} may be attributed to a small peripheral rim of tumor regrowth. The only slight increase in *k* might be due to the contribution of increased permeability through newly established blood vessels in the tumor.

By enabling differentiation between ADC_{high} and ADC_{perf}, diffusion-weighted MR imaging simultaneously provides information about tumor cell viability and tissue perfusion changes. Diffusion-weighted MR imaging is noninvasive and can be performed in patients in whom venous access is difficult. It also can be repeated at short intervals if necessary. In addition, it is cheaper than dynamic contrast-enhanced MR imaging because no contrast medium is injected and the examination time is shorter. Disadvantages are its lower spatial resolution and small distortion artifacts, which make exact localization of different areas more difficult. In addition, diffusion-weighted MR images might be more affected than are dynamic contrast-enhanced images by partial volume effects and movement artifacts.

Dynamic contrast-enhanced MR imaging has a high temporal resolution and thus allows better quantification of perfusion while it provides additional information about permeability (22). However, it does not permit differentiation between viable and necrotic tumor tissue. Dyke et al (20) showed a positive correlation between findings at dynamic contrast-enhanced MR imaging and the necrotic tumor fraction at histologic analysis in osteogenic sarcoma and Ewing sarcoma during and after induction chemotherapy. However, as chemotherapy directly destroys tumor cells, and because the pathologic correlation in the previously mentioned investigation was obtained 15 days after imaging was performed, all nonperfused areas found on dynamic contrast-enhanced MR images could be expected to be histologically necrotic. Nonperfused but viable tumor cells existing at the time of examination would predictably be histologically necrotic with such a delay in surgical removal and pathologic correlation. Dynamic contrast-enhanced MR imaging is minimally invasive. Short-term repetition of dynamic contrast-enhanced MR imaging may produce erroneous results due to trapping of contrast agent in the necrotic areas (19,25). In addition, postprocessing of the dynamic contrast-enhanced MR image data is more time consuming than analysis of the diffusion-weighted MR image data.

Our analysis of the entire tumor volume, without differentiation between viable and necrotic areas, may have been a shortcoming in our study. Analyzing the effect of vascular targeting agents on the entire tumor volume enabled a better comparison of the two different MR imaging methods. However, the different spatial resolution of the two methods did not allow accurate comparison of the center and periphery of the tumors between diffusion-weighted MR images and dynamic contrast-enhanced MR images. Small susceptibility-induced distortions on the diffusion-weighted MR images prevented such a comparison. In contrast, a failure to evaluate the entire tumor volume might result in sampling errors related to tumor heterogeneity, errors that are similar to those associated with invasive methods, because the sampled region may not be representative of the entire tumor (28). In addition, consideration of the entire tumor volume is less observer dependent. Information gathered from consideration of the entire tumor is also more readily applicable to an evaluation of treatment outcome.

Practical application: Dynamic contrast-enhanced MR imaging and diffusion-weighted MR imaging enable noninvasive assessment of the effects of vascular targeting agents on tumors. A good correlation was found between ADC_{perf} and other perfusion parameters (the volume transfer constant *k* and the initial slope of the contrast enhancement–time curve) in this study. The volume transfer constant *k* is more sensitive to smaller vascular changes, but only ADC_{high} provides information that enables differentiation between viable and necrotic tumor tissue.

References

1. Tozer GM, Prise VE, Wilson J, et al. Combretastatin A-4 phosphate as a tumor vascular-targeting agent: early effects in tumors and normal tissues. Cancer Res 1999; 59:1626–1634.
2. Tozer GM, Kanthou C, Parkins CS, Hill SA. The biology of the combretastatins as tumour vascular targeting agents. Int J Exp Pathol 2002;83:21–38.
3. Dark GG, Hill SA, Prise VE, Tozer GM, Pettit GR, Chaplin DJ. Combretastatin A-4, an agent that displays potent and selective toxicity toward tumor vasculature. Cancer Res 1997;57:1829–1834.
4. Maxwell RJ, Wilson J, Prise VE, et al. Evaluation of the anti-vascular effects of combretastatin in rodent tumours by dynamic contrast enhanced MRI. NMR Biomed 2002;15:89–98.
5. Siemann DW, Mercer E, Lepler S, Rojiani AM. Vascular targeting agents enhance chemotherapeutic agent activities in solid tumor therapy. Int J Cancer 2002;99:1–6.
6. Galbraith SM, Rustin GJ, Lodge MA, et al. Effects of 5,6-dimethylxanthenone-4-acetic acid on human tumor microcirculation assessed by dynamic contrast-enhanced magnetic resonance imaging. J Clin Oncol 2002;20:3826–3840.
7. Galbraith SM, Maxwell RJ, Lodge MA, et al. Combretastatin A4 phosphate has tumor antivascular activity in rat and man as demonstrated by dynamic magnetic resonance imaging. J Clin Oncol 2003;21: 2831–2842.
8. Rustin GJ, Bradley C, Galbraith S, et al. 5,6-dimethylxanthenone-4-acetic acid (DMXAA), a novel antivascular agent: phase I clinical and pharmacokinetic study. Br J Cancer 2003;88:1160–1167.
9. Rustin GJ, Galbraith SM, Anderson H, et al. Phase I clinical trial of weekly combretastatin A4 phosphate: clinical and pharmacokinetic results. J Clin Oncol 2003;21:2815–2822.
10. Anderson HL, Yap JT, Miller MP, Robbins A, Jones T, Price PM. Assessment of pharmacodynamic vascular response in a phase I trial of combretastatin A4 phosphate. J Clin Oncol 2003;21:2823–2830.
11. Dowlati A, Robertson K, Cooney M, et al. A phase I pharmacokinetic and translational study of the novel vascular targeting agent combretastatin a-4 phosphate on a single-dose intravenous schedule in patients with advanced cancer. Cancer Res 2002;62: 3408–3416.
12. Jameson MB, Thompson PI, Baguley BC, et al. Clinical aspects of a phase I trial of 5,6-dimethylxanthenone-4-acetic acid (DMXAA), a novel antivascular agent. Br J Cancer 2003;88:1844–1850.
13. Stevenson JP, Rosen M, Sun W, et al. Phase I trial of the antivascular agent combretastatin A4 phosphate on a 5-day schedule to patients with cancer: magnetic resonance imaging evidence for altered tumor blood flow. J Clin Oncol 2003;21:4428–4438.
14. Roth Y, Tichler T, Kostenich G, et al. High-*b*-value diffusion-weighted MR imaging for pretreatment prediction and early monitoring of tumor response to therapy in mice. Radiology 2004;232:685–692.
15. Le Bihan D, Breton E, Lallemand D, Aubin ML, Vignaud J, Laval-Jeantet M. Separation of diffusion and perfusion in intravoxel incoherent motion MR imaging. Radiology 1988;168:497–505.
16. Tofts PS, Berkowitz B, Schnall MD. Quantitative analysis of dynamic Gd-DTPA enhancement in breast tumors using a permeability model. Magn Reson Med 1995; 33:564–568.
17. Tofts PS. Modeling tracer kinetics in dynamic Gd-DTPA MR imaging. J Magn Reson Imaging 1997;7:91–101.
18. Thoeny HC, De Keyzer F, Chen F, et al. Diffusion-weighted MR imaging in monitoring the effect of a vascular targeting

agent on rhabdomyosarcoma in rats. Radiology 2005;234:756–764.
19. Padhani AR, Husband JE. Dynamic contrast-enhanced MRI studies in oncology with an emphasis on quantification, validation and human studies. Clin Radiol 2001;56:607–620.
20. Dyke JP, Panicek DM, Healey JH, et al. Osteogenic and Ewing sarcomas: estimation of necrotic fraction during induction chemotherapy with dynamic contrast-enhanced MR imaging. Radiology 2003;228: 271–278.
21. Beauregard DA, Thelwall PE, Chaplin DJ, Hill SA, Adams GE, Brindle KM. Magnetic resonance imaging and spectroscopy of combretastatin A4 prodrug-induced disruption of tumour perfusion and energetic status. Br J Cancer 1998;77:1761–1767.
22. Su MY, Jao JC, Nalcioglu O. Measurement of vascular volume fraction and blood-tissue permeability constants with a pharmacokinetic model: studies in rat muscle tumors with dynamic Gd-DTPA enhanced MRI. Magn Reson Med 1994;32:714–724.
23. Kremser C, Judmaier W, Hein P, Griebel J, Lukas P, de Vries A. Preliminary results on the influence of chemoradiation on apparent diffusion coefficients of primary rectal carcinoma measured by magnetic resonance imaging. Strahlenther Onkol 2003; 179:641–649.
24. Dzik-Jurasz A, Domenig C, George M, et al. Diffusion MRI for prediction of response of rectal cancer to chemoradiation. Lancet 2002;360:307–308.
25. Lang P, Wendland MF, Saeed M, et al. Osteogenic sarcoma: noninvasive in vivo assessment of tumor necrosis with diffusion-weighted MR imaging. Radiology 1998; 206:227–235.
26. Prise VE, Honess DJ, Stratford MR, Wilson J, Tozer GM. The vascular response of tumor and normal tissues in the rat to the vascular targeting agent, combretastatin A-4-phosphate, at clinically relevant doses. Int J Oncol 2002;21:717–726.
27. Tofts PS, Brix G, Buckley DL, et al. Estimating kinetic parameters from dynamic contrast-enhanced T(1)-weighted MRI of a diffusable tracer: standardized quantities and symbols. J Magn Reson Imaging 1999;10: 223–232.
28. Evelhoch JL. Key factors in the acquisition of contrast kinetic data for oncology. J Magn Reson Imaging 1999;10:254–259.